Environmental performance of nano-structured $Ca(OH)_2/TiO_2$ photocatalytic coatings for buildings

Manuel Nuño[1], Giovanni L. Pesce[1], Chris R. Bowen[2], Panayiotis Xenophontos[1], Richard J. Ball[1]*

[1]BRE Centre for Innovative Construction Materials, Department of Architecture and Civil Engineering, University of Bath, Claverton Down, BA2 7AY

[2]Department of Mechanical Engineering, University of Bath, Claverton Down, BA2 7AY

* Corresponding author

Abstract

This paper describes the environmental performance of a mixed phase coating (photocatalytic nanolime) manufactured from a colloidal nano-structured calcium hydroxide in alcohol (nanolime) combined with titanium dioxide. Titanium dioxide is commonly used as a photocatalytic material for self-cleaning coatings and environmental pollution control within the construction industry. Although currently nanolime and titania based materials are used separately, there is an increasing interest in the development of a photocatalytic nanolime coating. This paper reports the photocatalytic effect of titanium dioxide on the carbonation of nanolime and its influence on the degradation processes in polluted environments. A suspension of 25g/l of nanolime in ethanol and 7.4% wt/vol titanium dioxide was applied to specimens of Bath stone. For comparison, additional specimens were treated only with the nanolime. The specimens were exposed to oxides of nitrogen and sulphur under 30% RH for 120 hours. Exposure was carried out under both, UV and daylight. After exposure, the effect of titanium dioxide on the carbonation of nanolime and on the degradation processes was investigated using scanning electron microscopy (SEM), energy dispersive X-ray analysis (EDS) and X-ray photo electron spectroscopy (XPS). Results were evaluated considering the dissolution processes of the two oxides in water, and modelled using PHREEQC. Results show that the nanolime and the photocatalytic nanolime coatings promote reaction of SO_2. In addition, the photocatalytic effect of anatase promotes formation of a surface layer of calcium sulphate and inhibits carbonation of calcium hydroxide. The was attributed to the oxidation of sulphur dioxide to sulphur trioxide by hydroxyl radicals which led to the formation of sulphuric acid.

1. Introduction

Since the industrial revolution concentrations of the acid forming pollutants sulphur dioxide (SO_2) and nitrogen oxides (NO_x) have increased. This has resulted in the accelerated degradation of new and historic buildings in city centres and industrial areas. The introduction of more resistant materials and coatings to reduce these undesirable effects represent a challenge for the modern construction industry.

The processes of chemical decay of calcium carbonate ($CaCO_3$), which is one of the main constituents of limestone, has been the focus of numerous studies. The most aggressive chemical attack is mainly attributed to the oxides of sulphur and nitrogen. When SO_2 dissolves in water sulphurous acid (H_2SO_3) is formed whereas dissolution of SO_3 in water generates sulphuric acid (H_2SO_4). Both acids are strong enough to dissolve $CaCO_3$ contained in the stones or renders that are used as outer skins of buildings. Equations 1-7 show the proposed mechanism for sulfonation and the role of NO_2 in the oxidation of SO_2 [1], [2]:

$$SO_2 + H_2O \rightarrow H_2SO_3 \quad (1)$$

$$H_2SO_3 + CaCO_3 \rightarrow CaSO_3 + H_2CO_3 \quad (2)$$

$$SO_2 + NO_2 \rightarrow SO_3 + NO \quad (3)$$

$$SO_3 + H_2O \rightarrow H_2SO_4 \quad (4)$$

$$H_2SO_4 + CaCO_3 \rightarrow CaSO_4 + H_2CO_3 \quad (5)$$

$$NO + NO_2 + H_2SO_4 \rightarrow 2NOHSO_4 + H_2O \quad (6)$$

$$2NOHSO_4 + SO_2 + H_2O \rightarrow 3H_2SO_4 + 2NO \quad (7)$$

Sulfonation, however, is not the only process that can lead to chemical degradation of $CaCO_3$. This, in fact, can also be degraded by the products formed by the dissolution of NO_2 in water, as shown in equations 8-9 [3], [4]:

$$NO_2 + H_2O \rightarrow HNO_3 + HNO_2 \quad (8)$$

$$2HNO_3 + CaCO_3 \rightarrow Ca(NO_3)_2 + H_2CO_3 \quad (9)$$

In this work nanolime is examined as the calcium carbonate based material. Nanolime is as a colloidal suspension of nano-sized particles of calcium hydroxide ($Ca(OH)_2$) in an alcohol such as ethanol and isopropanol. It is commonly used as a consolidant in the field of cultural heritage [5]. The material acts as a binding agent of degraded surfaces because after application the $Ca(OH)_2$ reacts with the atmospheric carbon dioxide (CO_2) to produce $CaCO_3$. In contrast to building lime which is

formed by burning a source of calcium carbonate, nanolime is produced by precipitation. Nano-sized $Ca(OH)_2$ crystals are precipitated following mixing of supersaturated aqueous solutions of calcium chloride ($CaCl_2$) and sodium hydroxide (NaOH) under carefully controlled conditions. Following precipitation, water is substituted with alcohol to extend the long term stability of the nano sized $Ca(OH)_2$ crystals [6]. Precipitated crystals are plate-like with hexagonal shape and an aspect ratio of approximately 10:1. The average particle size is 150 nm (IBZ-Freiberg n.d.) although crystals can range from tens to several hundred nanometres [7]. The product was developed at the beginning of the new millennium as a consolidant for frescos [8], [9] and as de-acidification treatment for paper and canvas [10]. Later, however, its use extended to stone consolidation [6], [11] and as a nano-coating. When mixed with other materials such as titanium dioxide (TiO_2) the nanolime acts as a binding agent.

Titanium dioxide is the natural oxide of Ti^{+IV} which is a semiconductor with three main crystallographic structures. Anatase is one of the polymorphs and is widely studied for its photocatalytic properties when exposed to UV radiation. Previous researchers have investigated the use of titanium dioxide and its photocatalytic reactions in a wide range of applications such as water treatment [12]–[14], air purification [15]–[18] self-cleaning surfaces [19]–[24] or for the development of new super hydrophilic surfaces [20].

Photocatalysis is a chemical phenomenon observed in certain compounds that are able to absorb UV photons which in turn promote the migration of electrons from the conduction to the valence band, creating a charge separation. This separation produces a reactive hole (h_{vb}^+) and electron (e_{cb}^-) that can migrate to the surface of the material. At the surface the holes and electrons are able to participate in a photocatalytic process by adsorbing and reacting with molecules such as H_2O and O_2. This leads to the formation of free radicals as described by equations 10-15 [25]–[28].

$$TiO_2 + h\nu \rightarrow h_{vb}^+ + e_{cb}^- \quad (10)$$

$$h_{vb}^+ + H_2O \rightarrow \bullet OH + H^+ \quad (11)$$

$$e_{cb}^- + H^+ \rightarrow \bullet H \quad (12)$$

$$e_{cb}^- + O_2 \rightarrow O_2^{\bullet -} \quad (13)$$

$$h_{vb}^+ + O_2^{\bullet -} \rightarrow {}^1O_2 \quad (14)$$

$$H^+ + O_2^{\bullet -} \rightarrow HO_2^{\bullet} \quad (15)$$

This paper investigates the effect of a TiO_2 on the carbonation and sulphation of nanolime in SO_2 and NO_2 rich environments. Surfaces consisting of nano-particles of anatase mixed with nanolime were applied to specimens of Bath stone: a porous building limestone that has been used for centuries in the South West of the United Kingdom.

2. Experimental Method

All specimens used in this test were cut from a single piece of newly quarried Bath stone extracted from the Combe Down mines in Bath and North East Somerset, UK. The stone was cut into test specimens 5 x 10 x 10 mm where all surfaces were freshly cut (un-weathered). Each piece was individually cleaned with acetone and distilled water to remove impurities prior to being dried in an oven at 60ºC for 12 hours.

Three different specimens were used in each test: 1) a control specimen made of uncoated sound stone; 2) a specimen coated with nanolime and 3) a specimens coated with a mixture of nanolime and TiO_2.

Nanolime suspension was supplied by IBZ-Salzchemie GmbH & Co. KG (Germany) under the trade name CaLoSiL®. A product with a concentration of 25g/l in ethanol was used in all cases. Anatase in the form of Aeroxide® P25 was supplied by Sigma Aldrich (≥99.5% trace metals basis, average particle size 21 nm, surface area from $35m^2/g$ to $65m^2/g$). In order to obtain a stable colloidal suspension, 7.4% wt/vol Anatase was dispersed in CaLoSiL® just before the application and then sonicated for about 20 seconds.

The coating was applied by immersing the specimens in the suspensions for approximately 10 seconds. This allowed five sides of each specimen (main face of 10 x 10 mm and four sides of 5 x 10 mm) to be evenly covered. After immersion, the specimens remained in air at room temperature for several seconds to allow evaporation of the ethanol before being placed in the reactor at 25ºC.

Photocatalytic activity was evaluated for the specimens exposed to SO_2 under both UV and daylight radiation. UV radiation was obtained from a 4x4 array of 16 individual GaN UV-LEDs with a wavelength range of 376–387 nm and total intensity of 8 W/m^2. All other specimens were only exposed to daylight simulating external environmental conditions. The power of the light in the UVA range was 3 mW/m^2.

All specimens were exposed for 120 hours to atmospheres produced with: 1) artificial air containing 7 ppm SO_2; 2) artificial air containing 7 ppm NO_2; 3) artificial air containing 3.5 ppm SO_2 and 3.5 ppm NO_2. The concentration of pollutants was set to 7ppm in all the experiments; previous research showed optimum results after exposing to 5-10ppm pollutants [2], [29] as well RH remained constant at 7ppm exposure and 30% respectively. Table 1 shows details of the experimental conditions.

The cylindrical 3mm thick soda glass reactor with a diameter of 78mm used as a reactor in the tests is shown in Figure 1. The reactor contained two gas inlets, a gas outlet and a lid to facilitate introduction and removal of the specimens. The gas system that allowed production of specific atmospheres was designed in order to be able to introduce all the three gases at the same time. The desired gas compositions for the experiments were produced by introducing the following gases into the cell: 1) zero air grade (composition: 0.5 ppm H_2, 2 ppm He, 1 ppm CH_4, <5 ppm H_2O, 5 ppm Ne, ~20.95% O_2, 9300 ppm Ar, 385 ppm CO_2, 0.8 ppm N_2O, N_2 balance); 2) zero air grade containing 10.7 ppm of NO_2; 3) zero air grade containing 10.4 ppm of SO_2 in the appropriate proportions. All gases were supplied by BOC Gases Ltd. Each gas cylinder was connected to a gas flow meter capable of measuring gas flows from 5cm^3/min to 100cm^3/min with an accuracy of ±0.5ml/min (Platon Gap meter Type NGX supplied by Roxspur Measurement & Control Ltd). The gas from the zero air grade cylinders was humidified by passing it through a glass bubbler containing deaerated water before being passed into the cell. The other gas inlet of the cell was used to introduce the dry gas from the other two cylinders that were mixed using a three-way valve.

Figure 1 – Image of the glass reactor

Table 1 – Experimental conditions showing the gas flow and the RH of each experiment. Pollutant concentrations (in ppm) are calculated considering the initial concentration and the mixed volumes of gas. All the experiments were carried for five days, under the constant conditions.

Experiment number	Exposed pollutant	SO_2 flow (ml/min)	NO_2 flow (ml/min)	100% humid air (ml/min)	Light irradiation
1	7 ppm SO_2	22	-	10	Daylight cycles
2	7 ppm NO_2	-	22	10	Daylight cycles
3	3.5ppm SO_2 and 3.5 ppm NO_2	10	10	10	Daylight cycles
4	7 ppm SO_2 under UV	22	-	10	Constant 8W/m^2

3. PHREEQC modelling

To evaluate the experimental results, dissolution of SO_2, NO_2 and CO_2 in water was modelled using PHREEQC [38]. The program is based on equilibrium chemistry of aqueous solutions interacting with several phases, including gases. PHREEQC is routinely used in disciplines such as geochemistry, hydrology, environmental pollution, water treatment and the construction industry. PHREEQC has been used to simulate the ion–ion and the ion–solid interactions in the multi-ionic transport in concrete [30], [31], chemical degradation of concrete [32]–[34], dissolution processes of calcium-silicate-hydrate [35], [36], and phase and morphology evolution of $CaCO_3$ precipitated by carbonation of hydrated lime [37].

Simulations applied in this work were based on previously reported PHREEQC protocols [38]. Initial conditions consisted of 1 kg of pure water at 25 °C with pH=7 (this was set to be as an adjustable parameter to achieve charge balance). The equilibrium phases included two species: gas and solid. CO_2, SO_2 and NO_2 were considered as gas with the respective concentrations calculated according to Table 1 and the log of p_{CO2} (in bar) was set to simulate the different partial pressures. The number of moles considered was set to 100 to model the equilibrium with infinite reservoirs. Solid phases considered were modelled using an infinite number of moles and a saturation index (SI) of 0 so that these had to be in equilibrium with the solution at the end of the simulation. Simulations were performed with the thermodynamic data from the Lawrence Livermore National Laboratory database of Berkeley (the LLNL database built in PHREEQC). The PHREEQC input file used is shown in Algorithm 1.

4. Chemical and physical characterisation

Micro-morphologies of the Bath stone and coatings used in the tests were evaluated using a JEOL JSM64802V scanning electron microscope (SEM) with a working distance of 10 mm, an accelerating voltage of 15 kV and a spot size of 30 nm. Specimens were coated with a 20 nm thick layer of gold using an Edward Sputter S150B Coater to prevent surface charging. Energy Dispersive X-ray Spectroscopy (EDS) was performed on uncoated specimens using a working distance of 10 mm, accelerating Voltage of 25 kV and a spot size of 51 nm in high vacuum (25 MPa). Due to its penetration depth (1-2 μm), this technique was used to evaluate the degradation processes carried within the bulk of the coating.

The surface layers (within 1-10 nm) were characterized using X-ray Photoelectron Spectroscopy (XPS) using a Thermo Scientific Theta Probe with an AlK_{α} (1486 eV) X-ray source, operated at 100 W (Thermo Fisher Scientific Inc., Waltham, MA.) using a flood gun in an operating vacuum of 10^{-8} mbar. The adventitious hydrocarbon C1s peak at 284.8eV was used to correct the spectra for specimen charging. The software CASAXPS 2.3.16 RP 1.6 (Casa Software Ltd., Teingmouth, Devon, UK) was used for the peak fitting. The atomic percentage of each element detected was calculated from the peak areas, assuming a Shirley background and fitted using a Gaussian/Lorentzian ratio and asymmetry factors to give the best fit to the peaks. All the fitted peaks were normalized excluding the area of the adventitious carbon peak.

Wide scan survey spectra were obtained between 0 and 1400eV binding energy (BE) with pass energy of 200 eV and dwell time of 50 ms. In addition, scans of higher resolution were taken at different BE ranges with pass energy of 40 eV and dwell time of 100ms for C1s, N1s, O1s, S2p, Ca2p and Ti2p regions.

5. Results

5.1. PHREEQC simulation

Table 2 reports the activity of CO_3^{2-}, SO_4^{2-} and NO_2^- ions in pure water (i.e. no solid phase was introduced as the initial condition) as calculated by PHREEQC using different gas mixes and the model shown in Algorithm 1 (the simulation number is equivalent to the experiment number in table 1). The data show that in pure water, the activity of SO_4^{2-} ion is many orders of magnitude higher than the activity of NO_2^- and CO_3^{2-} ions in all conditions.

Table 2 - Activity of CO_3^{2-}, SO_4^{2-} and NO_2^- ions in pure water as calculated by the PHREEQC

Simulation number	Gas phases	Ion activity as calculated by PHREEQC		
		CO^{2-}_3	SO^{2-}_4	NO_2^-
1	385 ppm CO_2 7 ppm SO_2	1.047×10^{-24}	4.089×10^{-3}	-
2	385 ppm CO_2 7 ppm NO_2	2.700×10^{-24}	-	2.160×10^{-14}
3	385 ppm CO_2 3.5 ppm SO_2 3.5 ppm NO_2	8.872×10^{-26}	6.028×10^{-3}	8.203×10^{-15}

Table 3 shows the activity of CO_3^{2-}, SO_4^{2-} and NO_2^- ions when calcite is introduced as the main solid phase in contact with the solution. Calcite used in this model since it simulates the presence of $CaCO_3$ formed during the carbonation of nanolime. Results show that, as in pure water, the activity of the SO_4^{2-} ion is several order magnitudes higher than the activity of NO_2^- and CO_3^{2-} ions and that under these conditions Anhydrite ($CaSO_4$), Bassanite ($CaSO_4 \cdot 0.5H_2O$) and Gypsum ($CaSO_4 \cdot 2H_2O$) can be formed as solid phases.

Table 3 - Activity of CO_3^{2-}, SO_4^{2-} and NO_2^- ions in pure water in equilibrium with calcite and solid phases formed at the end of the simulation

Simulation set up			Ion activity			Solid phases formed
N.	Gas phases	Solid phases	CO^{2-}_3	SO^{2-}_4	NO_2^-	
1	CO_2 (385 ppm) SO_2 (7 ppm)	Calcite	8.031×10^{-9}	1.721×10^{-1}	-	$CaSO_4$ $CaSO_4 \cdot 0.5H_2O$ $CaSO_4 \cdot 2H_2O$
2	CO_2 (385 ppm) NO_2 (7 ppm)	Calcite	1.808×10^{-8}	-	2.463×10^{-11}	-
3	CO_2 (38 5ppm) SO_2 (3.5 ppm) NO_2 (3.5 ppm)	Calcite	9.270×10^{-9}	1.822×10^{-1}	1.594×10^{-11}	$CaSO_4$ $CaSO_4 \cdot 0.5H_2O$ $CaSO_4 \cdot 2H_2O$

Table 4 shows the activity of CO_3^{2-}, SO_4^{2-} and NO_2^- ions when both, calcite and Portlandite are included in the simulation. Portlandite used in this model simulates the presence of uncarbonated nanolime particles during the tests. The results show that, as well as in pure water, and in presence of

calcite, the activity of SO_4^{2-} ion is several orders of magnitude higher than the activity of NO_2^- and CO_3^{2-} ions. Furthermore, the results suggest that Anhydrite ($CaSO_4$), Bassanite ($CaSO_4 \cdot 0.5H_2O$) and Gypsum ($CaSO_4 \cdot 2H_2O$) are the only solid phases that could be formed at the end of the test.

Table 4 - Activity of CO_3^{2-}, SO_4^{2-} and NO_2^- ions in pure water in equilibrium with Calcite and Portlandite, and solid phases that could be produced at the end of the tests

Simulation set up			**Ion activity**			**Solid phases formed**
N.	**Gas phases**	**Solid phases**	**CO^{2-}_3**	**SO^{2-}_4**	**NO_2^-**	
1	CO_2 (385 ppm) SO_2 (7 ppm)	Calcite Portlandite	6.775×10^{-9}	7.822×10^{-2}	-	$CaSO_4$ $CaSO_4 \cdot 0.5H_2O$ $CaSO_4 \cdot 2H_2O$
2	CO_2 (385 ppm) NO_2 (7 ppm)	Calcite Portlandite	1.968×10^{-8}	-	1.672×10^{-9}	-
3	CO_2 (385 ppm) SO_2 (7 ppm) NO_2 (7 ppm)	Calcite Portlandite	1.063×10^{-8}	1.451×10^{-1}	1.032×10^{-9}	$CaSO_4$ $CaSO_4 \cdot 0.5H_2O$ $CaSO_4 \cdot 2H_2O$

5.2. SEM imagining

Figure 2 shows the surfaces of the control specimen (a), the specimen coated with nanolime (b) and the specimen coated with the nanolime-titania coating (c) after exposure to SO_2. Figure 2a shows the structure of Bath stone. A distributed set of clusters composed by Oolites makes the stone's structure very porous. Bath stone was previously characterized by mercury intrusion porosimetry (MIP) using a Micrometrics AutoPore III [39]. The mayority of the pores were around 10 and 0.1µm in diameter, and the macro pores were over 100µm and micropores (between oolites) which are between 10 and 1µm in diameter. Figure 2b illustrates the even distribution of nanolime on the surface and within the surface pores of the stone, covering the Oolites and making them invisible. Figure 2c shows Bath stone covered with a photocatalytic mixed phase nanolime coating. The presence of TiO_2 in the photocatalytic nanolime coating is not visible in the SEM images due to the limited magnification. Figure 2b and 2c show a coating with a high surface area. By comparing the coated and uncoated stone images the macropores are not blocked allowing gas and liquid vapour to diffuse into and out of the stone.

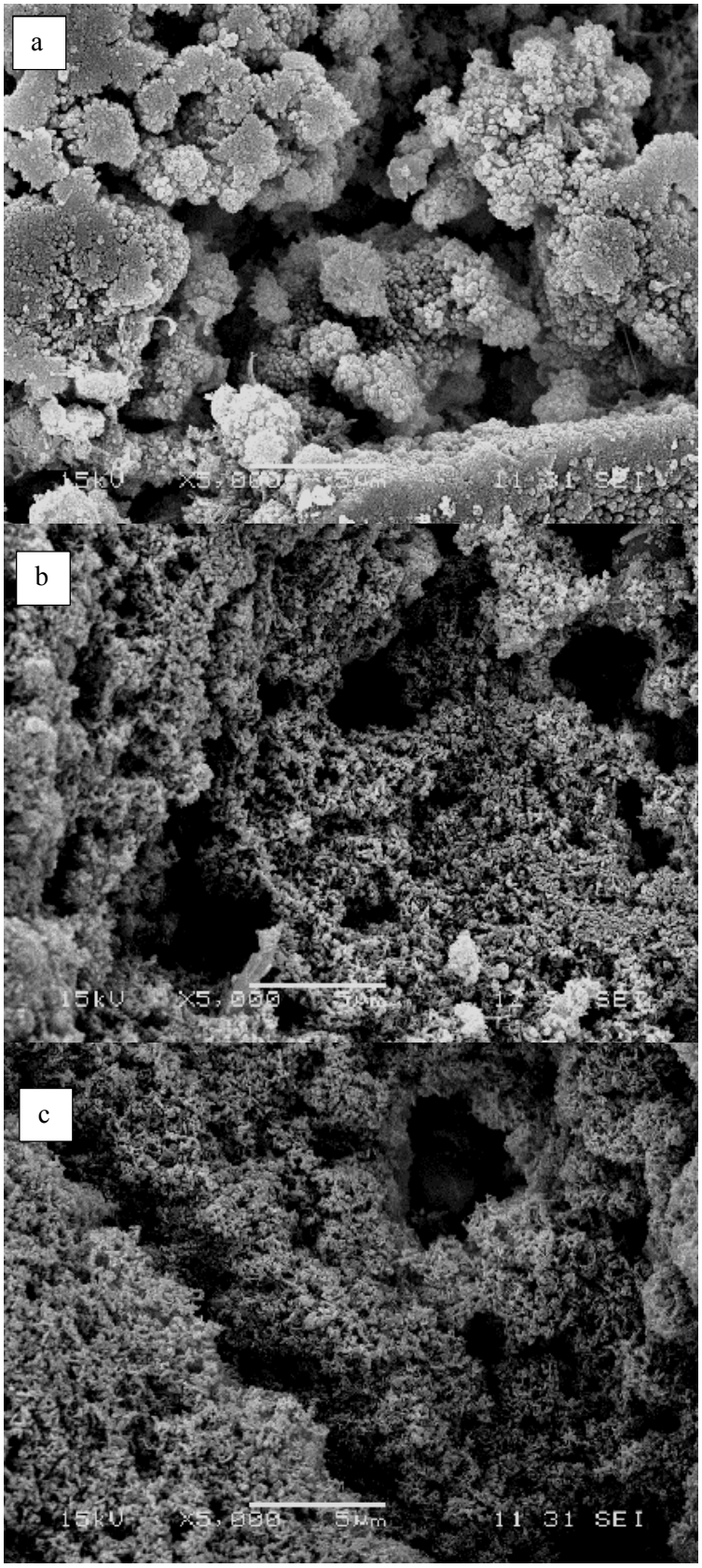

Figure 2 - SEM images of: a) uncoated Bath stone after SO_2 exposure; b) nanolime coated Bath stone specimen after SO_2 exposure; c) Bath stone treated with the photocatalytic nanolime coating after SO_2 exposure.

5.3. Energy dispersive X-ray spectroscopy (EDS)

Following exposure to the conditions in Table 1, quantitative analysis of the specimens was carried out using EDS, the results of which are shown in table 5. The data in the table is an average calculated from the results of five individual analyses, each carried out at a randomly selected representative location of the specimen surface.

Table 5 – Specimen composition determined by EDS spectroscopy on specimens following experimental conditioning exposure

	Specimen	**S (at. %)**	**Ti (at. %)**
7 ppm NO_2 33%RH Daylight cycles	Untreated	-	-
	Nanolime coating	-	-
	Photocatalytic Nanolime	-	4.4
7 ppm SO_2 33%RH Daylight cycles	Untreated	0.37	-
	Nanolime coating	2.36	-
	Photocatalytic Nanolime	1.77	7.12
3.5 ppm NO_2+3.5 ppm SO_2 33% RH Daylight cycles	Untreated	0.56	-
	Nanolime coating	0.34	-
	Photocatalytic Nanolime	1.68	4.4
7 ppm SO_2 33% RH UV-light	Untreated	0.72	-
	Nanolime coating	2.38	-
	Photocatalytic Nanolime	4.45	6.6

EDS analysis did not detect the presence of nitrogen based molecules in the surface of specimens exposed to 7 ppm of NO_2. Between 4.4 and 7.12 atomic percentage titanium was identified on the specimens coated with TiO_2 whereas no appreciable amount was detected on the other specimens. However in comparison to the specimen exposed to 7 ppm SO_2, results indicated the presence of sulphur, with higher values in the specimens coated with nanolime and photocatalytic nanolime. Exposure to the 3.5 ppm NO_2 and 3.5 ppm SO_2 gas mixture showed a reduction in the amount of sulphur detected on the nanolime coated specimen (0.34 atomic %), compared with the 7ppm SO_2 exposure, which was within the range of sulphur detected in the untreated specimens (0.37 and 0.56 atomic 5?%?). The photocatalytic nanolime coating showed 1.68 atomic % of sulphur which was comparable to the value of 1.77 atomic % obtained for the 7 ppm of SO_2.

5.4. X-ray photelectron spectroscopy results

The nature of the surface layer of the specimens after five days exposure was evaluated using XPS analysis, a survey spectra is shown in Figure 3. Binding energies and elemental ratios for carbon, nitrogen, oxygen, sulphur, calcium and titanium, calculated from higher resolution spectra in specific regions, are shown in Table 6.

The adventitious carbon contamination peak at 284.8eV was identified on all the specimens examined and used to calibrate the spectra for surface charging, however an additional peak corresponding to $CaCO_3$ was also identified. The binding energy of this peak ranged between 288.6 and 289.2eV which is in agreement with studies by Kang [40] and Demri [41] who report $CaCO_3$ binding energies of 288.6 and 289.2eV. The binding energy for the Ca 2p peak ranged between 346.3 and 347.5eV which is in accordance with previous studies by Ming [42] and Stipp [43] who reported $CaCO_3$ binding energies of 346.5 and 347.7eV.

The specimens exposed to 7 ppm NO_2 diluted in air did not show the presence of sulphur, indicating that no significant amount of sulphur was present in the specimen stone before testing, and that any sulphur detected on the surface of the specimens exposed to SO_2 originated from a surface reaction. Peaks corresponding to N 1s were identified between binding energies of 399.1 to 400.6eV, related to the presence of a carbon-nitrogen bond within an organic matrix [44]. In the spectral region corresponding to nitrate (N 1s 407.5eV) [45] no signal was detected suggesting that $Ca(NO_3)_2$ was not formed.

Binding energies for Ti 2p peaks varied between 458.1 and 459.0, and for O 1s the observed peaks are within the range of 528.8-529.5eV. These results agreed with studies carried by Dementjev [46] and Bedri [47], which identified Ti 2p binding energies from 458.0 to 459.4ev and for O 1s from 529.4 to 530.6eV. These were attributed to the TiO_2 in the coatings.

The XPS spectra of specimens exposed to 3.5 ppm NO_2 and 3.5 ppm SO_2 also showed S 2p 3/2 peaks at binding energies between 167.8 and 168.3 eV which corresponded to $CaSO_3$. Calculated atomic percentages of 0.5, 0.3 and 0.1 for the untreated, nanolime coating, and photocatalytic nanolimes were less than that observed on the specimens exposed to 7 ppm SO_2. These smaller concentrations may be attributed to the lower concentration of SO_2.

The XPS spectra from specimens exposed to 7 ppm SO_2 diluted in air at a relative humidity of 33% with daylight cycles all showed peaks corresponding to sulphur. The binding energies between 166.6 and 168.6 eV are in agreement with studies by Siriwardane and Hong [48], [49] and characteristic of calcium sulphite (SO_3^{2-}). Compositions of 1.0, 3.2 and 4.6 atomic % for the untreated (stone surface),

nanolime coating, and photocatalytic nanolime indicated that the nanolime is more reactive when compared to the stone substrate. This may be attributed to the higher solubility of $Ca(OH)_2$ compared to $CaCO_3$ and the higher surface area of the nanolime compared to stone.

The XPS spectra from specimens exposed to 7 ppm SO_2 diluted in air at 33% RH under UV light also showed peaks corresponding to sulphur. The binding energies between 168.4 and 168.6 eV observed for the nanolime and untreated stone are in agreement with studies by Siriwardane and Hong [48], [49] and characteristic of calcium sulphite (SO_3^{2-}). The atomic percentages of 2.2 and 4.0 are slightly higher, but still comparable with the equivalent specimens exposed to daylight cycles.

The specimen containing photocatalytic nanolime exposed to UVA had a Ca 2p binding energy of 348.2eV which was higher than values between 346.3 and 347.5 eV which was detected for all the other specimens. This is comparable to a Ca 2p binding energy of 348eV observed by Siriwarde [48] for calcium sulphate. A higher binding energy for S 2p 3/2 of 169.9eV, compared to values ranging between 167.8 and 168.6 eV, is also in agreement with previous research by Moulder et al. [44] who observed a binding energy of 169.4eV for sulphate. The difference in behaviour of the photocatalytic nanolime under UV irradiation is illustrated in Figure 4 which shows the spectra over the S 2p range for the nanolime coated specimen and photocatalytic nanolime. A shift of approximately 2eV is observed between the S 2p peaks of nanolime coating and photocatalytic coating. On nanolime $CaSO_3$ was observed whereas for the photocatalytic coating $CaSO_4$ was generated.

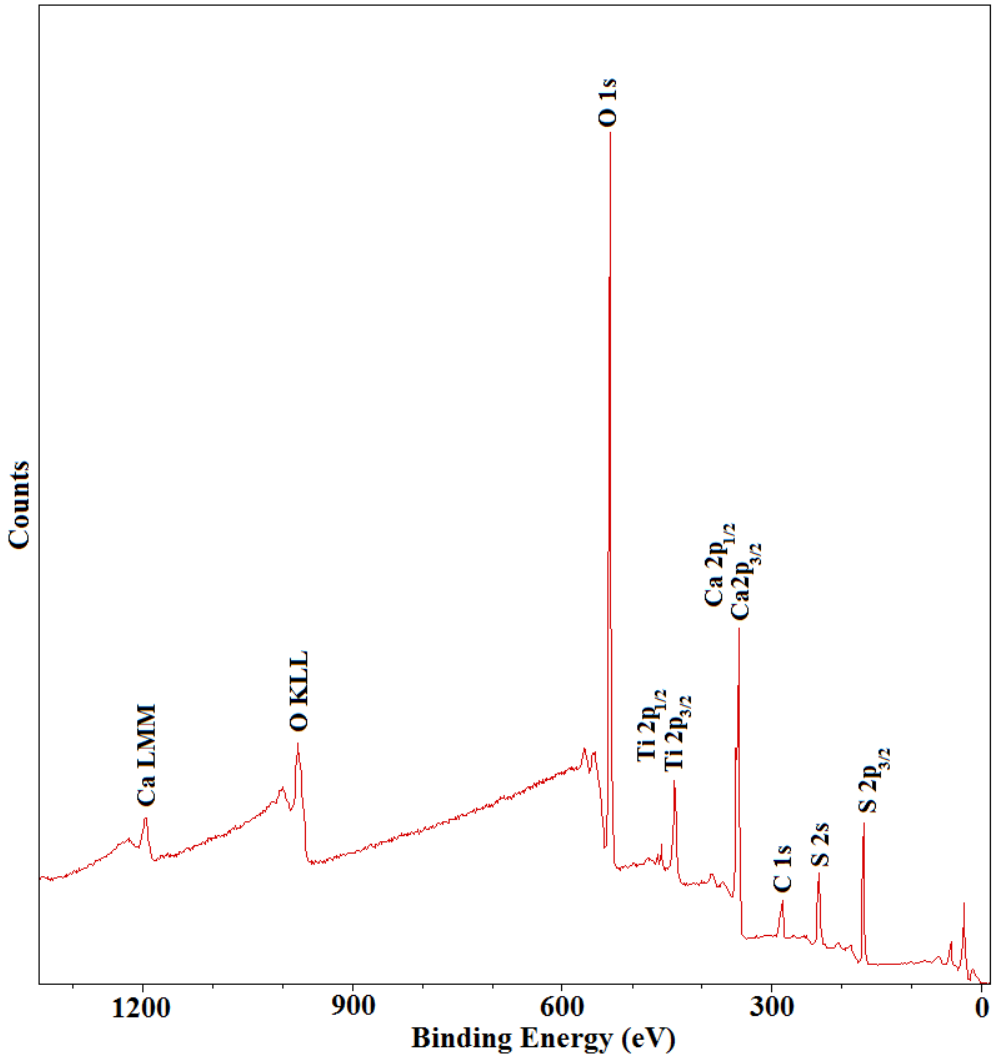

Figure 3 – Typical wide scan survey XPS spectrum for photocatalytic nanolime coated Bath stone after five days exposure to 7 ppm SO_2 under UV irradiation

Table 6 – Binding energies and relative concentration in atomic percent of carbon, nitrogen, oxygen, sulphur, calcium and titanium obtained from XPS analysis

Experimental conditions	Specimen ID	**Binding energy, eV**/Relative concentration in atomic %							
		C 1s	**N 1s**	**O 1s**		**S $2p_{3/2}$**		**Ca $2p_{3/2}$**	**Ti $2p_{3/2}$**
		CO_3^{2-}	**Organic matrix**	**CO_3^{2-}**	**TiO_2**	**SO_3^{2-}**	**SO_4^{2-}**		**TiO_2**
7 ppm NO_2 33% RH Daylight cycles	Untreated	**288.6/** 3.3	**399.5/** 0.9	**531.5/**78.8	-	-	-	**346.4/**17.0	-
	Nanolime coating	**289.1/** 4.3	**399.2/** 0.2	**531.3/**59.9	-	-	-	**346.8/**35.6	-
	Photocatalytic Nanolime	**288.8/** 3.5	**399.3/** 0.4	**530.9/**54.5	**528.8/**1.7	-	-	**346.6/**28.4	**458.1/** 11.5
7 ppm SO_2 33% RH Daylight cycles	Untreated	**288.9/**5.0	**399.3/** 0.6	**531.0/**65.0	-	**167.9/** 1.0	-	**346.3/**28.4	-
	Nanolime coating	**288.7/** 4.4	**399.1/** 0.2	**530.9/**56.4	-	**166.6/** 3.2	-	**346.4/**35.8	-
	Photocatalytic Nanolime	**288.8/** 1.0	**399.1/** 0.2	**532.0/**62.4	-	**168.6/** 4.6	-	**347.3/**27.1	**459.0/** 4.6
3.5 ppm NO_2+3.5 ppm SO_2 33% RH Daylight cycles	Untreated	**288.8/** 3.1	**399.7/** 1.0	**531.7/**77.9	-	**167.9/** 0.5	-	**346.7/**17.5	-
	Nanolime coating	**289.0/** 5.0	**399.8/** 0.4	**530.8/**58.7	-	**167.8/** 0.3	-	**346.3/**35.6	-
	Photocatalytic Nanolime	**289.1/**3.4	**399.2/** 0.1	**531.0/**53.3	**528.9/**3.1	**168.3/** 0.1	-	**346.7/**27.0	**458.9/** 13.0
7 ppm SO_2 33% RH UV exposure	Untreated	**288.8/** 3.3	**399.7/** 0.9	**531.7/**69.4	-	**168.6/** 2.2	-	**346.9/**24.2	-
	Nanolime coating	**289.0/** 2.1	**400.6/** 0.1	**532.2/**66.1	-	**168.4/** 4.0	-	**347.5/**27.7	-
	Photocatalytic Nanolime	**287.8/** 0.7	**400.2/** 0.1	**532.4/**50.9	**529.5/**6.9	-	**169.4/** 8.2	**348.2/**24.1	**459.0/** 9.1

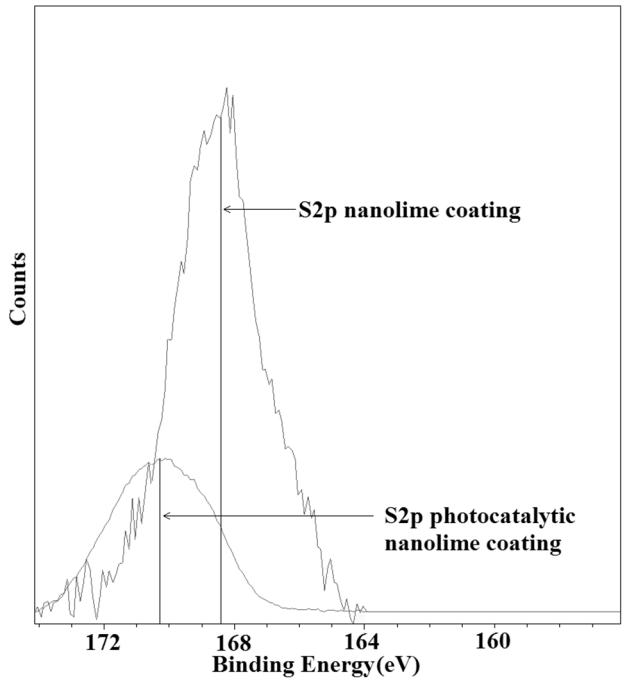

Figure 4 –XPS spectra of sulphur $2p_{3/2}$ region for nanolime and photocatalytic nanolime coated Bath stone after five days exposure to 7 ppm SO_2 under UV irradiation.

6. Discussion

The combined results given by EDS and XPS reveal a difference in the elemental concentration between the bulk of the coating (1-2 μm) and the surface layer (maximum 10 nm). The concentration of CO_2 in the gas mixture was approximately 55 times higher than that of the NO_2 and SO_2, however the concentration of sulphur compounds detected on the surface was similar to the $CaCO_3$ detected. Simulations using PHREEQ suggest that, because of the very low activity of the NO_2^- ion in aqueous solution only the solid phases produced by the interaction of SO_2 with the system should be detected at the end of the experiments.

For the experiment that exposed specimens to 7 ppm of NO_2, the exposure did not affect the composition within the bulk; it is possible that the gas concentration or the activity of nitrogen ions was too low to produce phases detectable by EDS. In addition, XPS showed a small amount of organic matrix in the outermost layer.

The formation of $CaSO_4$ on the surface of carbonate containing materials historically used in construction, such as limestone, is widely accepted. However previous research, under atmospheric conditions, by Chin [50] describes the formation of $CaSO_4$ as a two stage process involving the initial formation of $CaSO_3$ (IV) which is followed by further oxidation to sulphate (VI) [50]. The rate of these two reactions is dependent on the local water and oxygen concentrations.

Analysis of the S 2p 3/2 binding energies obtained for the XPS spectra from the specimens indicated the presence of SO_3^{2-} in the form of calcium sulphite. This phase was identified on the uncoated limestone surface in addition to nanolime and photocatalytic nanolime surfaces. The concentration of sulphur on surfaces coated with nanolime and photocatalytic nanolime was three times higher than that on the stone surface due to the presence of more reactive $Ca(OH)_2$ and the associated higher surface area. EDS indicated a six-fold increase, the higher value compared to XPS, was attributed to the greater penetration depth of the analysis into the specimen surface.

The addition of anatase P25 to the nanolime, increased the surface area and the absorption of SO_2 and NO_x onto the outermost layer of material. When the photocatalytic nanolime coating was exposed to UV irradiation, XPS revealed the presence of SO_4^{2-} as calcium sulphate. Compared to all the other specimens examined the amount of $CaCO_3$ detected was considerably lower.

The presence of calcium sulphate suggests reaction with sulphuric acid opposed to sulphurous acid. Margitan [51] demonstrated that a hydroxyl radical can initiate the oxidation of SO_2 into SO_3 as described by equations 14-16. This radical is known to readily form on the surface of photocatalysts such as anatase under illumination with UV light [26]–[28].

$$SO_2 + \bullet OH \rightarrow HOSO_2\bullet \qquad (14)$$

$$HOSO_2\bullet + \bullet OH \rightarrow H_2O + SO_3 \qquad (15)$$

Sulphuric acid can form by the reaction of SO_3 with water as shown in equation 16, however reaction with the hydroxyl radical has also been shown to lead to the formation of sulphuric acid as in equation 17.

$$SO_3 + H_2O \rightarrow H_2SO_4 \qquad (16)$$

$$SO_2 + 2\bullet OH \rightarrow H_2SO_4 \qquad (17)$$

When the sulphuric acid is formed, it reacts with $Ca(OH)_2$ and $CaCO_3$ as shown in equations 18 and 19 to form calcium sulphate.

$$H_2SO_4 + Ca(OH)_2 \rightarrow 2H_2O + CaSO_4 \qquad (18)$$

$$H_2SO_4 + CaCO_3 \rightarrow CaSO_4 \qquad (19)$$

7. Conclusions

This study provides an insight into the effect of photocatalysis in the carbonation process of nanolime and in its degradation process when exposed to SO_2.

There was no evidence of nitration under exposure to 7 ppm NO_2. XPS data indicated the binding energies of the N1s peak were characteristic of N-C bonds in an organic matrix. The concentration of nitrogen deposited was increased when the gas composition consisted of 3.5 ppm of SO_2 and 3.5 ppm of NO_2.

In the case of the specimens coated with nanolime the results show a preferential reaction of $Ca(OH)_2$ with SO_2 relative to CO_2, which is further enhanced in presence of anatase and UV light. Under these conditions the majority of the $Ca(OH)_2$ reacts with SO_2 to form calcium sulphate, and only a small amount reacted with CO_3^{2-} to form $CaCO_3$. Results show the presence of anatase increased the deposition of sulphur and nitrogen when the specimens were exposed to 7 ppm of SO_2 and UV light, and the $CaSO_4$ generated reduced carbonation. This was attributed to the oxidation of SO_2 to SO_3 by hydroxyl radicals generated on the surface of nano-anatase thus forming sulphuric acid opposed to sulphurous acid. Results from the photocatalytic nanolime formulation suggest they could be used to reduce atmospheric pollutant levels through creation of a sacrificial layer. This would prevent further damage to the limestone façade and could be applied cities where pollution is detrimental to historic buildings.

8. Acknowledgement

The authors acknowledge research funding from a University of Bath Research Studentship and the Engineering and Physical Sciences Research Council (EPSRC) through project EP/K025597/1. Thanks are also due to the National EPSRC XPS Users' Service, hosted by nanoLAB at the University of Newcastle, UK, in particular Dr Anders Barlow. The authors are grateful to Professor W. N. Wang for specifying the UV-LED source and to Dr John Mitchels and Ursula Potter for assistance with EDS spectroscopy and SEM imaging.

9. Appendix

Algorithm 1 – PHREEQC model used to simulate the dissolution of CO_2, NO_2 and SO_2 and water with and without solid phases. The code shows the model used to simulate the dissolution of 7 ppm of SO_2 and 385 ppm of CO_2 in pure water and in absence of solid phases as initial conditions (hashtags inform the software to ignore the code lines where these are located). For each condition described in table 1, the gas phases, the gas concentrations and the solid phases were modified by commenting or un-commenting the code with a hashtag.

```
SOLUTION 1
   temp      25
   pH        7 charge
   pe        4
   redox     pe
   units     mol/kgw
   density   1
   Alkalinity 0
   -water    1 # kg
EQUILIBRIUM_PHASES 1
#   Calcite 0 1000
#   Portlandite 0 1000
   CO2(g)    -3.408822658 100
#   NO2(g)    -5.149185348 100
   SO2(g)    -5.149185349 100
END
```

10. References

[1] A. Lancia, D. Musmarra, and F. Pepe, "Modeling of SO2 Absorption into Limestone Suspensions," *Ind. Eng. Chem. Res.*, vol. 36, no. 1, pp. 197–203, Jan. 1997.

[2] G. C. Allen, A. El-Turki, K. R. Hallam, D. McLaughlin, and M. Stacey, "Role of NO2 and SO2 in degradation of limestone," *Br. Corros. J.*, vol. 35, no. 1, pp. 35–38, Jan. 2000.

[3] Y.-N. Lee and S. E. Schwartz, "Evaluation of the rate of uptake of nitrogen dioxide by atmospheric and surface liquid water," *J. Geophys. Res. Ocean.*, vol. 86, no. C12, pp. 11971–11983, Dec. 1981.

[4] P. Kirkitsos and D. Sikiotis, "Deterioration of Pentelic marble, Portland limestone and Baumberger sandstone in laboratory exposures to NO2: A comparison with exposures to gaseous HNO3," *Atmos. Environ.*, vol. 30, no. 6, pp. 941–950, Mar. 1996.

[5] L. Dei and B. Salvadori, "Nanotechnology in cultural heritage conservation: nanometric slaked lime saves architectonic and artistic surfaces from decay," *J. Cult. Herit.*, vol. 7, no. 2, pp. 110–115, Apr. 2006.

[6] V. Daniele and G. Taglieri, "Nanolime suspensions applied on natural lithotypes: The influence of concentration and residual water content on carbonatation process and on treatment effectiveness," *J. Cult. Herit.*, vol. 11, no. 1, pp. 102–106, Jan. 2010.

[7] V. Daniele, G. Taglieri, and R. Quaresima, "The nanolimes in Cultural Heritage conservation: Characterisation and analysis of the carbonatation process," *J. Cult. Herit.*, vol. 9, no. 3, pp. 294–301, Jul. 2008.

[8] R. Giorgi, L. Dei, and P. Baglioni, "A New Method for Consolidating Wall Paintings Based on Dispersions of Lime in Alcohol," *Stud. Conserv.*, vol. 45, no. 3, pp. 154–161, Sep. 2000.

[9] P. Baglioni and R. Giorgi, "Soft and hard nanomaterials for restoration and conservation of cultural heritage," *Soft Matter*, vol. 2, no. 4, pp. 293–303, 2006.

[10] R. Giorgi, L. Dei, M. Ceccato, C. Schettino, and P. Baglioni, "Nanotechnologies for Conservation of Cultural Heritage: Paper and Canvas Deacidification," *Langmuir*, vol. 18, no. 21, pp. 8198–8203, Sep. 2002.

[11] P. López-Arce, L. S. Gomez-Villalba, L. Pinho, M. E. Fernández-Valle, M. Á. de Buergo, and R. Fort, "Influence of porosity and relative humidity on consolidation of dolostone with calcium hydroxide nanoparticles: Effectiveness assessment with non-destructive techniques," *Mater. Charact.*, vol. 61, no. 2, pp. 168–184, Feb. 2010.

[12] A. Fujishima, X. Zhang, and D. A. Tryk, "TiO2 photocatalysis and related surface phenomena," *Surf. Sci. Rep.*, vol. 63, no. 12, pp. 515–582, 2008.

[13] S.-A. Lee, K.-H. Choo, C.-H. Lee, H.-I. Lee, T. Hyeon, W. Choi, and H.-H. Kwon, "Use of Ultrafiltration Membranes for the Separation of TiO2 Photocatalysts in Drinking Water Treatment," *Ind. Eng. Chem. Res.*, vol. 40, no. 7, pp. 1712–1719, Mar. 2001.

[14] J. Ryu and W. Choi, “Substrate-Specific Photocatalytic Activities of TiO2 and Multiactivity Test for Water Treatment Application,” *Environ. Sci. Technol.*, vol. 42, no. 1, pp. 294–300, Nov. 2007.

[15] J. Kolarik and J. Toftum, “The impact of a photocatalytic paint on indoor air pollutants: Sensory assessments,” *Build. Environ.*, vol. 57, no. 0, pp. 396–402, 2012.

[16] G. Hüsken, M. Hunger, and H. J. H. Brouwers, “Experimental study of photocatalytic concrete products for air purification,” *Build. Environ.*, vol. 44, no. 12, pp. 2463–2474, Dec. 2009.

[17] G. Ramakrishnan and A. Orlov, “Development of novel inexpensive adsorbents from waste concrete to mitigate NOx emissions,” *Build. Environ.*, vol. 72, pp. 28–33, Feb. 2014.

[18] A. M. Ramirez, K. Demeestere, N. De Belie, T. Mäntylä, and E. Levänen, “Titanium dioxide coated cementitious materials for air purifying purposes: Preparation, characterization and toluene removal potential,” *Build. Environ.*, vol. 45, no. 4, pp. 832–838, 2010.

[19] Y. Ohko, S. Saitoh, T. Tatsuma, and A. Fujishima, “Photoelectrochemical Anticorrosion and Self-Cleaning Effects of a TiO2 Coating for Type 304 Stainless Steel ,” *J. Electrochem. Soc.* , vol. 148 , no. 1 , pp. B24–B28, Jan. 2001.

[20] Z. Wu, D. Lee, M. F. Rubner, and R. E. Cohen, “Structural Color in Porous, Superhydrophilic, and Self-Cleaning SiO2/TiO2 Bragg Stacks,” *Small*, vol. 3, no. 8, pp. 1445–1451, Aug. 2007.

[21] Y. Paz, Z. Luo, L. Rabenberg, and A. Heller, “Photooxidative self-cleaning transparent titanium dioxide films on glass,” *J. Mater. Res.*, vol. 10, no. 11, pp. 2842–2848, 1995.

[22] E. I. Cedillo-González, R. Riccò, M. Montorsi, M. Montorsi, P. Falcaro, and C. Siligardi, “Self-cleaning glass prepared from a commercial TiO2 nano-dispersion and its photocatalytic performance under common anthropogenic and atmospheric factors,” *Build. Environ.*, vol. 71, pp. 7–14, Jan. 2014.

[23] A. Chabas, S. Alfaro, T. Lombardo, A. Verney-Carron, E. Da Silva, S. Triquet, H. Cachier, and E. Leroy, “Long term exposure of self-cleaning and reference glass in an urban environment: A comparative assessment,” *Build. Environ.*, vol. 79, pp. 57–65, Sep. 2014.

[24] A. Chabas, T. Lombardo, H. Cachier, M. H. Pertuisot, K. Oikonomou, R. Falcone, M. Verità, and F. Geotti-Bianchini, “Behaviour of self-cleaning glass in urban atmosphere,” *Build. Environ.*, vol. 43, no. 12, pp. 2124–2131, Dec. 2008.

[25] A. Fujishima and K. Honda, “Electrochemical photolysis of water at a semiconductor electrode,” *Nature*, vol. 238, no. 5358, pp. 37–38, 1972.

[26] A. Z. Fujishima X., “Titanium dioxide photocatalysis: present situation and future approaches,” *Comptes Rendus Chim.*, vol. 9, no. 5–6, pp. 750–760, 2006.

[27] A. Fujishima, T. N. Rao, and D. A. Tryk, “Titanium dioxide photocatalysis,” *J. Photochem. Photobiol. C Photochem. Rev.*, vol. 1, no. 1, pp. 1–21, 2000.

[28] O. Carp, C. L. Huisman, and A. Reller, “Photoinduced reactivity of titanium dioxide,” *Prog. Solid State Chem.*, vol. 32, no. 1–2, pp. 33–177, 2004.

[29] G. C. Allen, A. El-Turki, K. R. Hallam, D. McLaughlin, and M. Stacey, "Role of NO2 and SO2 on the degradation of limestone," in *Stone deterioration in polluted urban environments*, vol. 3, D. J. Mitchell and D. E. Searle, Eds. CRC publisher, 2004, pp. 119–130.

[30] Y. Elakneswaran, A. Iwasa, T. Nawa, T. Sato, and K. Kurumisawa, "Ion-cement hydrate interactions govern multi-ionic transport model for cementitious materials," *Cem. Concr. Res.*, vol. 40, no. 12, pp. 1756–1765, Dec. 2010.

[31] P. . Brown and A. Doerr, "Chemical changes in concrete due to the ingress of aggressive species," *Cem. Concr. Res.*, vol. 30, no. 3, pp. 411–418, Mar. 2000.

[32] D. Jacques, L. Wang, E. Martens, and D. Mallants, "Modelling chemical degradation of concrete during leaching with rain and soil water types," *Cem. Concr. Res.*, vol. 40, no. 8, pp. 1306–1313, Aug. 2010.

[33] D. Sugiyama, "Chemical alteration of calcium silicate hydrate (C–S–H) in sodium chloride solution," *Cem. Concr. Res.*, vol. 38, no. 11, pp. 1270–1275, Nov. 2008.

[34] M. Moranville, S. Kamali, and E. Guillon, "Physicochemical equilibria of cement-based materials in aggressive environments—experiment and modeling," *Cem. Concr. Res.*, vol. 34, no. 9, pp. 1569–1578, Sep. 2004.

[35] C. S. Walker, D. Savage, M. Tyrer, and K. V. Ragnarsdottir, "Non-ideal solid solution aqueous solution modeling of synthetic calcium silicate hydrate," *Cem. Concr. Res.*, vol. 37, no. 4, pp. 502–511, Apr. 2007.

[36] F. X. Yao, M. C. Arbestain, S. Virgel, F. Blanco, J. Arostegui, J. A. Maciá-Agulló, and F. Macías, "Simulated geochemical weathering of a mineral ash-rich biochar in a modified Soxhlet reactor.," *Chemosphere*, vol. 80, no. 7, pp. 724–32, Aug. 2010.

[37] Ö. Cizer, C. Rodriguez-Navarro, E. Ruiz-Agudo, J. Elsen, D. Van Gemert, and K. Van Balen, "Phase and morphology evolution of calcium carbonate precipitated by carbonation of hydrated lime," *J. Mater. Sci.*, vol. 47, no. 16, pp. 6151–6165, 2012.

[38] C. A. J. Appelo and D. Postma, *Geochemistry, Groundwater and Pollution, Second Edition*. Boca Raton, FL: CRC Press/Taylor & Francis, 2005, p. 683.

[39] G. L. Pesce, D. Morgan, D. Odgers, A. Henry, M. Allen, and R. J. Ball, "Consolidation of weathered limestone using nanolime," *Proc. ICE - Constr. Mater.*, vol. 166, pp. 213–228, 2013.

[40] I.-C. Kang, Q. Zhang, S. Yin, T. Sato, and F. Saito, "Preparation of a visible sensitive carbon doped TiO2 photo-catalyst by grinding TiO2 with ethanol and heating treatment," *Appl. Catal. B Environ.*, vol. 80, no. 1–2, pp. 81–87, Apr. 2008.

[41] B. Demri and D. Muster, "XPS study of some calcium compounds," *J. Mater. Process. Technol.*, vol. 55, no. 3–4, pp. 311–314, Dec. 1995.

[42] M. Ni and B. D. Ratner, "Differentiation of Calcium Carbonate Polymorphs by Surface Analysis Techniques – An XPS and TOF-SIMS study," *Surf. Interface Anal.*, vol. 40, no. 10, pp. 1356–1361, Oct. 2008.

[43] S. L. Stipp and M. F. Hochella, “Structure and bonding environments at the calcite surface as observed with X-ray photoelectron spectroscopy (XPS) and low energy electron diffraction (LEED),” *Geochim. Cosmochim. Acta*, vol. 55, no. 6, pp. 1723–1736, Jun. 1991.

[44] J. F. Moulder, W. F. Stickle, P. E. Sobol, and K. D. Bomben, *Handbook of X-ray photoelectron Spectroscopy*. Eden Prairie: Perkin-Elmer Corporation, 1992.

[45] A. B. Christie, J. Lee, I. Sutherland, and J. M. Walls, “An XPS study of ion-induced compositional changes with group II and group IV compounds,” *Appl. Surf. Sci.*, vol. 15, no. 1–4, pp. 224–237, Apr. 1983.

[46] A. P. Dementjev, “Altered layer as sensitive initial chemical state indicator∗,” *J. Vac. Sci. Technol. A Vacuum, Surfaces, Film.*, vol. 12, no. 2, p. 423, Mar. 1994.

[47] B. Erdem, R. A. Hunsicker, G. W. Simmons, E. D. Sudol, V. L. Dimonie, and M. S. El-Aasser, “XPS and FTIR Surface Characterization of TiO2 Particles Used in Polymer Encapsulation,” *Langmuir*, vol. 17, no. 9, pp. 2664–2669, May 2001.

[48] R. V Siriwardane and J. M. Cook, “Interactions of SO2 with sodium deposited on CaO,” *J. Colloid Interface Sci.*, vol. 114, no. 2, pp. 525–535, Dec. 1986.

[49] H. Lu and P. G. Smirniotis, “Calcium Oxide Doped Sorbents for CO2 Uptake in the Presence of SO2 at High Temperatures,” *Ind. Eng. Chem. Res.*, vol. 48, no. 11, pp. 5454–5459, Jun. 2009.

[50] T. Chin, R. Yan, and D. T. Liang, “Study of the Reaction of Lime with HCl under Simulated Flue Gas Conditions Using X-ray Diffraction Characterization and Thermodynamic Prediction,” *Ind. Eng. Chem. Res.*, vol. 44, no. 23, pp. 8730–8738, Nov. 2005.

[51] J. J. Margitan, “Mechanism of the atmospheric oxidation of sulfur dioxide. Catalysis by hydroxyl radicals,” *J. Phys. Chem.*, vol. 88, no. 15, pp. 3314–3318, Jul. 1984.